HHS Public Access

Author manuscript

Mol Pharm. Author manuscript; available in PMC 2019 May 31.

Published in final edited form as:

Mol Pharm. 2019 May 06; 16(5): 1864–1873. doi:10.1021/acs.molpharmaceut.8b01148.

Magnetophoretic delivery of a tumor priming agent for chemotherapy of metastatic murine breast cancer

Jinho Park[1,2], **Joonyoung Park**[1], **Mark A. Castanares**[2], **David S. Collins**[2], and **Yoon Yeo**[1,3,*]

[1]Department of Industrial and Physical Pharmacy, Purdue University, 575 Stadium Mall Drive, West Lafayette, IN 47907, USA

[2]Lilly Research Laboratories, Lilly Corporate Center, Eli Lilly and Company, Indianapolis, IN 46285, USA

[3]Weldon School of Biomedical Engineering, Purdue University, 206 South Martin Jischke Drive, West Lafayette, IN 47907, USA

Abstract

Tumor microenvironment (TME) is a significant physical barrier to effective delivery of chemotherapy into solid tumors. To overcome this challenge, tumors are pre-treated with an agent that reduces cellular and extracellular matrix densities prior to chemotherapy. However, it also comes with a concern that metastasis may increase due to the loss of protective containment. We hypothesize that timely priming at the early stage of primary tumors will help control metastasis. To test this, we primed orthotopic 4T1 breast tumors with a paclitaxel (PTX)-loaded iron oxide decorated poly(lactic-co-glycolic acid) nanoparticle composite (PTX@PINC), which can be quickly concentrated in target tissues with the aid of an external magnet, and monitored its effect on the delivery of subsequently administered NPs. Magnetic resonance imaging and optical whole-body imaging confirmed that PTX@PINC was efficiently delivered to tumors by the external magnet and help loosen the tumors to accommodate subsequently-delivered NPs. Consistently, the primed tumors responded to Doxil better than non-primed tumors. In addition, lung metastasis was significantly reduced in the animals PINC-primed prior to Doxil administration. These results support that PINC combined with magnetophoresis can facilitate timely management of primary tumors with a favorable secondary effect on metastasis.

Keywords

Tumor priming; metastasis; paclitaxel; magnetic drug delivery; polymer-iron oxide nanocomposite

1. Introduction

For effective delivery of chemotherapy to solid tumors, physical barriers of tumor microenvironment (TME) need to be overcome.[1–5] TME features abnormal physiological

*Corresponding author: Yoon Yeo, Ph.D., Phone: 765.496.9608, Fax: 765.494.6545, yyeo@purdue.edu.

Supporting Information

The Supporting Information is available free of charge on the ACS Publications website.

Supporting Table and Figures

characteristics that impair interstitial transport of drug and nanomedicine. Uncontrolled cell growth induces high stress within the tumor and compresses blood and lymphatic vessels to interfere with drug perfusion and drainage of the interstitial fluid.[6] In addition, abnormal blood vessel networks driven by overactivation of proangiogenic pathways lead to the formation of tortuous and leaky vasculature, resulting in slow blood flow, increased blood viscosity and interstitial accumulation of fluid and macromolecules.[7] Coupled with the impaired lymphatic drainage, the fluid and macromolecules increase the interstitial pressure, reducing the transvascular and intratumoral pressure gradient, hindering the convective transport of a drug.[8] Moreover, the tumor extracellular matrix (ECM), comprising high levels of fibrous proteins and glycosaminoglycans, further deters diffusional transport of a drug.[1] These features of TME in concert generate significant challenges in effective chemotherapy of solid tumors.

To overcome the barriers in intratumoral drug delivery, chemotherapy has been combined with various pretreatments that reduce the cellular and ECM densities as well as transvascular and interstitial pressure gradients in tumors ("tumor priming").[2, 3] The pretreatments include enzymes, radiotherapy, hyperthermia, or metronomic chemotherapy.[1, 4] For example, collagenase and cathepsin C were used to digest collagen and decorin, respectively, resulting in significant increase in intratumoral diffusion of macromolecular dextran.[9] In addition, PEGylated hyaluronidase (PEGH20) has been used to degrade hyaluronic acid accumulated in solid tumors and increase tumor access of anti-cancer therapeutics in preclinical models and clinical trials.[10, 1112] Alternatively, 4-methylumbelliferone (MU) or its prodrug have been used to inhibit HA synthesis and improve liposomal delivery to 4T1 murine breast tumors.[13] With the same principle, losartan, a small molecule angiotensin II receptor blocker, increased intratumoral delivery of chemotherapy (Doxil® or 5-fluorouracil) in orthotopic models of pancreatic cancer by reducing the collagen I level in tumors.[14, 15] Radiotherapy has also shown to increase intratumoral accumulation of macromolecules or nanomedicines, including liposomal doxorubicin[16] and paclitaxel-loaded nanoparticles.[17] It is thought that radiation played multiple roles, such as increasing the pressure gradient, inducing tumor cell apoptosis and shrinkage,[16] and increasing transvascular permeability.[18] In addition, a tumor-penetrating peptide, iRGD, has shown to increase vascular and tissue permeability.[19, 20] iRGD binds to peritumoral endothelium via $\alpha\nu$ integrins and undergoes proteolytic cleavage to produce tumor penetrating CRGDK/R peptide, which enhances intratumoral transport of bystander drugs.[20] Chemotherapeutic drugs are also used to reduce the tumor cell density, expand the interstitial space, and enhance the penetration of subsequently administered drugs or nanoparticles. In particular, paclitaxel (PTX), an inhibitor of microtubule disassembly, has been used as a pretreatment to induce the apoptosis of cancer cells prior to the standard chemotherapy.[21, 22] PTX priming enhanced the delivery of doxorubicin-loaded liposomes to tumors with minimal distribution in normal tissues, facilitating tumor regression and prolonging the survival of model animals.[22] A study performed in a mouse model of human pancreatic cancer shows that PTX priming enhanced intratumoral delivery of gemcitabine by depleting peritumoral desmoplastic stroma.[23]

With the expected benefits of priming strategies in chemotherapy of tumors, a potential concern raised in tandem is that the relief of intratumoral transport barriers may increase

metastatic spread of primary tumor cells.[24] While considered a significant barrier to drug delivery, desmoplastic stroma is also viewed as a protective containment of tumor cells, which upon removal may unleash primary tumors with metastatic potential.[24] It is shown in genetically-engineered mouse models of pancreatic cancer that the depletion of tumor stroma rather led to reduced survival with increased epithelial-to-mesenchymal transition, stem cell-like phenotype, and metastasis.[25, 26] We hypothesize that timely tumor priming may however reduce the risk of metastasis through effective initial management of primary tumors. To test this, we perform tumor priming prior to chemotherapy with a polymer-iron oxide nanocomposite (PINC), which can be quickly concentrated at the target tissues with the aid of external magnet,[27] and monitor its effect on the progression of tumor with high metastatic potential.

In this study, we employed magnetophoretic delivery of PTX-loaded PINC (PTX@PINC) to reduce tumor stroma and evaluated its efficacy in enhancing the delivery of subsequent chemotherapy and managing the metastasis of orthotopic 4T1 tumor. Clinical utility of magnetophoresis remains controversial due to the limitations in the strength of magnetic field gradients; nevertheless, it is an excellent tool to control the localization of nanoparticles in animal models. Based on this merit, PTX@PINC was magnetophoretically delivered to tumor-bearing mice, and its tumor distribution was monitored with magnetic resonance imaging. The tumor priming effect of PTX@PINC was evaluated at both microscopic and macroscopic levels via tissue observation and optical whole-body imaging. The effect of priming on chemotherapy of tumors was evaluated in an orthotopic 4T1 breast cancer model to reveal that the chemotherapy combined with PINC-mediated tumor priming attenuated the growth of primary 4T1 tumors and suppressed lung metastasis.

2. Materials and Methods

2.1. Materials

Poly(lactic-co-glycolic acid) (PLGA) (lactic acid:glycolic acid=50:50, 4 kDa, ester endcap) and PLGA (lactic acid:glycolic acid=85:15, 30 kDa, ester endcap) were purchased from Lactel Absorbable Polymers (Birmingham, AL, USA). PLGA (lactic acid:glycolic acid=85:15, 150 kDa, acid endcap) was purchased from Akina, Inc. (West Lafayette, IN, USA). Methoxy-polyethylene glycol (2000 Da)-amine (MeO-PEG_{2000}-NH_2) was purchased from Nanocs Inc. (New York, NY, USA). Liposomal doxorubicin was purchased from Avanti Polar Lipids (Alabaster, AL, USA). 1,1’-Dioctadecyl-3,3,3’,3’-Tetramethylindotricarbocyanine Iodide (DiR) was purchased from Fisher Scientific (Hampton, NH, USA). Dopamine HCl was purchased from Alfa Aesar (Ward Hill, MA, USA). 3-(4,5-Dimethylthiazol-2-yl)-2,5-diphenyltetrazolium bromide (MTT) and Hoechst 33342 were purchased from Invitrogen (Eugene, OR, USA). All other reagents were purchased from Sigma-Aldrich (St. Louis, MO, USA).

2.2. Preparation and characterization of NPs

Preparation of PTX@PLGA NPs coated with polydopamine (PTX@PLGA–pD NPs)—PTX-loaded PLGA NPs (PTX@NP) were prepared with three different PLGA polymers by the single-emulsion method. Briefly, 50 mg of PLGA (4, 30 or 150 kDa) was

dissolved in 4 mL of CH_2Cl_2 and mixed with 50 μL of 5 wt% PTX (i.e., 2.5 mg) in $CHCl_3$. The PTX/PLGA mixture was added to 10 mL of 4 wt% polyvinyl alcohol (PVA) in water, and emulsified by a probe sonicator (Sonics Vibracell, Newtown, CT, USA) for 2 min in ice, pulsing at a power level of 7W and a 2:1 duty cycle every 6 sec. The emulsion was added to 20 mL of deionized (DI) water and stirred for 1 h, and the organic solvent was removed by rotary evaporation for 1 h. The resulting PTX@NP was collected by centrifugation at 16,000 rcf for 20 min at 4 °C and washed twice with DI water. For preparation of DiR-loaded PLGA NPs (DiR@NP), DiR were dissolved in the organic phase with PLGA at a target DiR content of 0.25 wt%.

An aqueous suspension of 0.1 wt% PTX@NP (1 mL) was mixed with an equal volume of 0.1 wt% dopamine HCl in Tris buffer (10 mM, pH 8.5). The mixture was incubated on an orbital shaker for 3 h at room temperature to coat the NP surface with a layer of polydopamine (pD). The pD-coated NP (NP-pD) was collected by centrifugation at 16,000 rcf for 20 min at 4 °C and re-dispersed as a 2 wt% suspension.

Preparation of polydopamine-coated Fe_3O_4 particles (IO–pD)—Colloidal Fe_3O_4 was synthesized as described previously[27] and collected by a handheld NeFeB magnet, washed 3 times with DI water, and dried in air. Freshly prepared Fe_3O_4 particles (4 mg) were added to 0.1 wt% dopamine HCl in Tris buffer (4 mL) and gently mixed for 30 min. The pD-coated Fe_3O_4 particles (IO-pD) were collected by a handheld magnet, re-dispersed as 0.4 wt% solution in fresh Tris buffer, and used immediately.

Preparation and characterization of PTX loaded polymer–iron oxide nanocomposites (PTX@PINC)—A suspension of 2 wt% PTX@NP-pD (1 mL) was added to four volumes of 0.1 wt% fresh dopamine HCl in Tris buffer (10 mM, pH 8.5), followed by one volume of 0.4 wt% IO–pD in Tris buffer (10 mM, pH 8.5). The mixture was agitated for 2 h by vortex mixing at room temperature and homogenized with a probe sonicator for 5 min (50% duty cycle every 4 s). The PLGA NP/Fe_3O_4 composites (PTX@NP-pD-IO) were collected with a handheld magnet and redispersed as a 2 wt% suspension in fresh Tris buffer (10 mM, pH 8.5). The PTX@NP-pD-IO suspension (3 mL) was mixed with 1 mL of 2 wt% MeO-PEG_{2000}-NH_2 solution in Tris buffer and agitated with a vortex mixer for 3 h at room temperature, followed by sonication for 2 min (50% duty cycle every 4 sec). The PEGylated PTX@NP-pD-IO composites (PTX@NP-pD-IO-PEG; i.e. PTX@PINC) were collected by applying a handheld magnet for 10 min, which was long enough to collect PTX@PINC but not enough to attract free IO-pD. The collected PTX@PINC was redispersed in DI water and stored at 4 °C.

2.3. Characterization of PTX@PINC

The hydrodynamic diameter of PTX@PINC was measured in DI water, and the zeta potential in phosphate buffer (2.5 mM, pH 7.4) by dynamic light scattering (DLS) using a Malvern Zetasizer Nano ZS90 (Malvern, Worcestershire, UK). NPs were visualized by transmission electron microscopy (TEM) using a Tecnai F20 (FEI, Hillsboro, OR, USA) with negative staining by 2% phosphotungstic acid. Scanning electron microscope with energy dispersive x-ray spectroscopy (SEM-EDX) was performed by an Oxford INCA

Energy 250 system (Oxford Instruments plc, UK). EDX data was analyzed by the AZtecOne software (Oxford Instruments plc, UK). To confirm the presence of PEG to PINC, PTX@PINC was dissolved in 50% acetonitrile and analyzed by matrix-assisted laser desorption-ionization mass spectroscopy (MALDI-MS) using a Voyager-DE PRO MALDI-MS (Applied Biosystems, Foster City, CA). MeO-PEG_{2000}-NH_2 was treated and analyzed in the same manner as a reference. The PTX loading efficiency was determined by HPLC after retrieving PTX from PTX@PINCs with acetonitrile. The iron content was determined by atomic absorption spectroscopy (AAS) using a Perkin-Elmer 3110 Spectrometer (Waltham, MA, USA). The DiR loading was determined by measuring the fluorescence of NP solution in acetonitrile with a Spectral AMI Optical Imaging System (Spectral Instruments, Tucson, AZ, USA).

2.4. PTX release from PTX@PINCs

The release kinetics of PTX from PTX@PINCs were evaluated in phosphate-buffered saline (PBS) containing 0.2% Tween 80 (PBST). Briefly, 1 mg of PTX@PINCs were suspended in 1 mL 0.2% PBST and incubated at 37 ℃ with rotation. At predetermined time points (up to 80 h), the NP suspension was centrifuged at 16,000 rcf for 10 min. The PTX concentration in each supernatant was measured with no other treatment. The remaining pellet was analyzed in the same manner as the PTX loading content determination.

2.5. Cytotoxicity of PTX@PINCs after short-term magnet-aided exposure

The cytotoxicity of PTX@PINCs was evaluated with 4T1 murine breast cancer cells (ATCC, Manassas, VA, USA) with or without an external magnet. 4T1 cells were seeded in a 96-well plate at a density of 10,000 cells per well in 200 μL of complete medium, grown overnight, and treated with PTX@PINCs equivalent to 0.85 μM PTX. An external magnet (8 mm) was placed under each well for 5 min. Subsequently, the medium was removed, and the cells were rinsed with fresh medium once. After additional 24 h incubation in the particle-free medium, the medium was replaced with 100 μL of fresh medium containing 75 μg of MTT reagent and incubated for 3.5 h, followed by the addition of the stop/solubilization solution. The absorbance of solubilized formazan crystals was read by a SpectraMax M3 microplate reader (Molecular Devices, Sunnyvale, CA, USA) at a wavelength of 562 nm. The measured sample absorbance was normalized to that of untreated control cells.

2.6. MR imaging of magnetophoretic delivery of PTX@PINC

All animal procedures were approved by Purdue Animal Care and Use Committee, in conformity with the NIH guidelines for the care and use of laboratory animals. Five to six week-old female Balb/c mice were purchased from Envigo (Indianapolis, IN, USA) and acclimatized for 1 week prior to the procedure. Each mouse received a subcutaneous injection of 5×10^5 4T1 cells in both flanks. When the average tumor volume reached 100–200 mm^3, animals were injected with 1 mg of PTX@PINCs (30 kDa) equivalent to 1.6 mg PTX/kg via tail vein. Immediately after injection, a handheld magnet ($G = 1$ kG/cm) was placed on one of the tumors for 30 min. MR images were acquired under 3% isoflurane anesthesia before and after PTX@PINC administration and magnet treatment. The time interval between two imaging events was approximately 2 h. Axial views of whole-body MR images were obtained using a 7-T small-animal MRI scanner. T_2*-weighted MR images

were obtained using a gradient echo sequence (TR/TE = 1781/15 msec, FOV = 32 mm^2, flip angle = 90°/180°, matrix size = 256 × 256, NEX = 4, number of slices = 40, and section thickness = 1 mm). T_2*-weighted datasets were processed by the ImageJ software (1.47v, Bethesda, MD, USA).

2.7. Optical whole-body imaging of DiR@NP distribution in PTX@PINC-primed tumors

The mice received intravenous injection of DiR@NPs (1 mg NP/mouse) at 12 h post-injection of PTX@PINCs, and the distribution of DiR fluorescence was monitored by the AMI imaging system ($\lambda_{Ex}/\lambda_{Em}$: 745 nm/790 nm). At 6 h post-injection of DiR@NPs, mice were sacrificed by CO_2 asphyxiation, and *ex vivo* image of tumors were taken by the AMI imaging system. The radiance (photon emission per unit area) of a region-of-interest (ROI) was calculated by the AMI viewer image software.

2.8. Acellular area induced by PTX@PINC injection

The tumor priming effect of PTX@PINC was evaluated by measuring the acellular area in tumor tissues. One milligram of PTX@PINC was injected to 4T1 tumor bearing mice by intravenous injection when the tumor size reached 100 mm^3. After 24 h, mice were sacrificed, and tumors were excised, fixed in 10% formalin solution, and sectioned in paraffin blocks for hemotoxylin and eosin (H&E) staining. The H&E-stained tissue section was examined by a confocal microscope with a 4× objective (Nikon America Inc., Melville, NY). For each section, 6–12 images were obtained and stitched by the Nikon NIS-Elements software. The acellular area in each tumor section (2–3 section per each side in each animal) was defined as the areas devoid of cells. The area was quantified by the Image J. Tumor area was first defined by a continuous outline, and acellular areas were determined within the outline according to the color threshold. % acellular area was defined as formula: % acellular area = acellular area/total tumor area ×100.

2.9. Antitumor efficacy study of Doxil after tumor priming by PTX@PINC

Liposomal doxorubicin (Doxil) was administered to orthotopic 4T1 tumor bearing mice intravenously 12 h after PTX@PINC priming of tumors. 1.5×10^5 cells in 50 μL of PBS was inoculated in the mammary fat pad.[28] When the tumors grew to 100–150 mm^3, animals were randomly assigned to 5 treatment groups: (i) the control group receiving PBS, (ii) PTX@PINC/magnet-primed but no Doxil (P/M/-), (iii) PTX@PINC with no magnet followed by Doxil (P/-/D), (iv) PTX@PINC/magnet-primed followed by Doxil (P/M/D), and (v) Doxil given prior to PTX@PINC/magnet-priming (D/P/M) with the same interval (12 h). PTX@PINC was given at a dose equivalent to 1.6 mg/kg PTX, and Doxil at 10 mg/kg doxorubicin. Doxil shows dose dependent tumor accumulation and anti-tumor efficacy.[29] Accordingly, the mice were treated with a total of two cycles of priming and treatment schedule to afford a measurable difference from the control groups. Tumor volume and body weight were monitored every other day. The length (L) and width (W) of each tumor were measured with a digital caliper, and the volume (V) was calculated per the modified ellipsoid formula: $V = (L \times W^2)/2$.[30] Specific growth rate of a tumor was calculated as $\Delta \log V/\Delta t$ (V: volume in mm^3, t: time in days).[31]

On day 33 post-inoculation, mice were sacrificed, and primary tumors in the mammary fat pad were excised and weighed. The lungs were excised, filled with dilute India ink solution through the trachea, destained in Fatake's solution, and fixed in 4% paraformaldehyde.[32–34] The number of metastatic nodules were counted.

2.10. Statistical analysis

Statistical analysis was performed with GraphPad Prism 7 (La Jolla, CA, USA). Data were analyzed by unpaired t-test, Kruskal-Wallis one-way ANOVA followed by Dunn's multiple comparisons test or ordinary one-way ANOVA followed by Tukey's multiple comparisons test. A value of $p < 0.05$ was considered statistically significant.

3. Results and Discussion

3.1. Synthesis and characterization of paclitaxel-loaded PINC

The schematic of PTX@PINC preparation is shown in Fig. 1a. Briefly, PTX-loaded PLGA NPs (PTX@NP) were prepared by the single emulsion method. The surface of PTX@NP was coated with polymerized dopamine (to form PTX@NP-pD) and mixed with polydopamine-coated iron oxide particles (IO-pD). PTX@NP-pD appeared to preferentially interact with IO-pD than with other PTX@NP-pD, likely due to relatively robust pD coating of iron oxide particle based on its metallic nature.[35–37] Finally, the IO-pD-covered PTX@NP-pD (PTX@NP-pD-IO) was stabilized by MeO-PEG_{2000}-NH_2 to form PTX@NP-pD-IO-PEG (PTX@PINC).

The PLGA NPs and iron oxide particles were pre-coated with pD layer to facilitate the surface modification. The pD layer is formed by oxidation of dopamine in weak alkaline condition, deposits on various solid surfaces including PLGA and iron oxide particles, and accommodates functional ligands with amine or thiol groups via Michael addition and/or Schiff base reactions.[35, 38, 39] In the formation of PINC, pD serves as an adhesive layer and helps to immobilize the iron oxide particles as well as MeO-PEG-NH_2 on the PLGA NPs.[27] Consistent with our earlier studies,[38, 40, 41] the pD coating was evident from the dark color of PTX@NP-pD, characteristic of polymerized dopamine, as well as the thin layer on the particle surface shown in the TEM image (Fig. 1b). The presence of iron oxide particles and PEG on PTX@PINC was confirmed by SEM-EDX analysis (Fig. 1c) and MALDI-MS (Fig. 1d, Figure S1), respectively. The TEM images of PTX@PINC showed dense iron oxide particles attached on the NP surface (Fig. 1b, Fig. S2a), clearly distinguished from PTX@NP-pD-PEG (NPs containing all other components except for iron oxide nanoparticles, Fig. S2b) or IO@NP-pD-PEG (NPs containing iron oxide particles inside the PLGA NP matrix, Fig. S2c). PTX@NP and PTX@NP-pD showed similar sizes in both DLS (Table 1) and TEM measurements (Fig. 1b), indicating that the pD layer had little contribution to the particle size. However, the Z-average of PTX@PINC was substantially larger than that of PTX@NP-pD (Table 1), partly due to the surface-bound iron oxide particles and also to the slight aggregation, which might not have been completely prevented by surface PEGylation. PTX@PINC maintained a constant size and surface-bound iron oxide particles in 50% FBS (Fig. S3a, b). The iron oxide particles persisted on the PINC surface after exposure to shear stress induced by vortex mixing and 28G needle passing (Fig.

S3c). These results suggest that PTX@PINC should survive protein-rich condition and shear stress during circulation.

3.2. *In vitro* release kinetics of PTX@PINC

To identify a formulation suitable for *in vivo* application, PTX@PINC was prepared with three types of PLGAs differing in the molecular weight (MW) or LA:GA ratio of PLGA. The morphology, size, and zeta potential of PTX@PINC were not significantly affected by the MW or LA:GA ratio of the polymers (Fig. S4, Table S1). The PTX loading ranged from 1.5 wt% to 2 wt%, with PTX@PINC made of higher MW PLGA showing slightly higher loading efficiency. The release kinetics of PTX from the three PTX@PINCS was monitored in PBST for 24 h to test the ability to retain drug during the initial circulation, the most critical period for tumor distribution of PTX@PINC. The drug release kinetics differed with the MW and composition of PLGA (Fig. S5a): PTX@PINC made of PLGA (4 kDa, LA:GA=50:50) showed burst release of PTX and 90% of drug release in 5 h, whereas those made of PLGA (150 kDa, LA:GA=85:15) showed a slower profile with 20% of the drug released in 24 h. PTX@PINC made of PLGA (30 kDa, LA:GA=85:15) showed an intermediate drug release profile. Given that the initial drug release from polymeric NPs represents diffusion-based transport,[42] the differential PTX release is attributable to the difference in hydrophobicity of the polymers, which determines the rate of hydration and swelling of the NP matrix. Since the drug prematurely released in circulation is likely to cause systemic side effects, PTX@PINC made of PLGA (4 kDa, LA:GA=50:50) with the high initial burst release was considered least desirable. Between PTX@PINCs made of PLGA (150 kDa, LA:GA=85:15) and PLGA (30 kDa, LA:GA=85:15), the latter releasing more drug toward 24 h was considered more favorable for inducing the priming effect. The PTX@PINC (30 kDa PLGA) continued to release PTX beyond 24 h, reaching 43% release by 80 h (Fig. S5b); however, the release rate is likely suboptimal for effective tumor priming. The drug release rate toward the later time points remains to be improved in the future studies.

3.3. *In vitro* magnetophoretic delivery of PTX@PINC

The effect of an external magnet on cellular delivery of PTX was evaluated with 4T1 cells. The cells were exposed to PTX@PINC with (+M) or without an external magnet (-M) for 5 min, and the cell viability was assessed after additional 24 h incubation in treatment-free medium (Fig. S5c). PTX@PINC made of PLGA (30 kDa, LA:GA=85:15) or PLGA (150 kDa, LA:GA=85:15) showed minimal cytotoxicity in the -M condition, consistent with the sustained drug release profile. Both types of PTX@PINC induced significant cytotoxicity in the +M condition. This indicates that PTX@PINC entered or adhered to the cells during the 5 min magnet exposure and released PTX during the additional incubation time. Meanwhile, PTX@PINC made of PLGA (4 kDa, LA:GA=50:50) showed greater toxicity than the previous two types, irrespective of the magnet application, suggesting that its toxicity was governed by the burst-released PTX. It is interesting that PTX@PINC (PLGA 4 kDa) was more toxic than free PTX, unlike others made of higher MW PLGAs, in the -M condition. Since blank PINC counterpart was non-toxic in the same condition, this difference may be attributable to the enhanced drug exposure by the cellular contact of NPs,[43] which can help concentrate the drug to the cells. The cytotoxicity study complements the release kinetics

results, confirming that PTX@PINC (PLGA 4 kDa) releasing PTX prematurely is undesirable for systemic application. PTX@PINC (PLGA 30 kDa) and PTX@PINC (PLGA 150 kDa) were comparable in cytotoxicity test, but PTX@PINC (30 kDa) was chosen for the subsequent *in vivo* studies of magnetophoretic tumor priming since it released PTX better than the latter in the later period.

3.4. *In vivo* imaging of magnetophoretic tumor priming

The tumor priming effect of magnetophoretically-delivered PTX@PINC was evaluated with female Balb/c mice bearing 4T1 tumors. 4T1 tumor cells were subcutaneously inoculated on both flanks of each mouse. Optimal tumor priming with PTX is reported to be 1 h infusion of 5 mg/kg PTX followed by 16 – 24 h interval prior to the main treatment.[21] We chose a lower dose of PTX (1.6 mg/kg PTX) and a shorter interval (12 h) than the reported optimum to distinguish the effect of the priming effect due to quick magnetophoretic delivery of PTX via PINC[27] from that of PTX released in circulation during the prolonged interval. The animals received PTX@PINC (equivalent to 1.6 mg/kg PTX) by tail-vein injection, and an external magnet was applied on one of the two tumors (Fig. 2a). MR imaging showed greater accumulation of PTX@PINC on the magnet-treated tumor (+M) than untreated side (-M), evidenced by greater T2-signal enhancement (darker field) on +M tumor (Fig. 2b, Fig. S6), consistent with our previous report.[27] To observe if magnetophoretically delivered PTX@PINC enhances the delivery of subsequently administered therapy, DiR@NP with an average diameter of ~200 nm (as a model NP therapy) was administered by intravenous injection at 12 h after the PTX@PINC treatment and monitored by whole-body fluorescence imaging over 6 h (Fig. 2c, Fig. S6). Three of five mice showed higher DiR signal at +M tumors than -M tumors, one showed similar signal, and one showed an opposite trend (Fig. 2d). Consistently, *ex vivo* images showed higher DiR fluorescence intensity at +M tumors than –M tumors (Fig. 2e) except for the one outlier. Although the result shows some degree of variability, the trend supports our hypothesis that tumor priming by magnetophoretically delivered PTX@PINC may enhance the accumulation of subsequently administered drugs.

3.5. Analysis of PTX@PINC-primed tumors

For mechanistic understanding of the enhanced NP delivery to PTX@PINC-primed tumors, tumor sections were sampled at 24 h post-PTX@PINC injection. According to the image analysis, the fraction of acellular area was significantly greater in +M tumors than in -M tumors (Fig. 3, Fig. S7). The MR imaging and tissue analysis collectively suggest that magnetophoretic delivery of PTX@PINC to tumors enhance the local effect of PTX on tumors, reducing the tumor density. The increased acellular area (Fig. 3) may have facilitated the intratumoral transport of subsequently administered DiR@NP (Fig. 2c–e).

3.6. Antitumor effect of Doxil after tumor priming by PTX@PINCs

To determine if tumor priming with PTX@PINC with an external magnet enhances the anticancer effect of subsequently delivered chemotherapy, Doxil (liposomal doxorubicin) was administered following the magnetophoretic delivery of PTX@PINC to orthotopic 4T1 tumor-bearing Balb/c mice (Fig. 4a). When tumor volume reached 100–150 mm^3 (on 10 d post-tumor inoculation), PTX@PINC (equivalent to 1.6 mg/kg PTX) was administered by tail vein injection followed by a 30 min magnet exposure to the tumor. 12 h after

PTX@PINC priming, Doxil (equivalent to 10 mg/kg doxorubicin) was administered by tail vein injection (designated as P/M/D, standing for PTX@PINC, Magnet, and Doxil). In addition to non-treatment control, regimens omitting Doxil or magnet (P/M/- or P/-/D), as well as an identical treatment in a scrambled order (D/P/M), were included as control treatments. The treatment cycle was repeated on 12 d post-tumor inoculation. As shown in Fig. 4b and c, P/M/D regimen was more effective than other control groups in attenuating the growth of primary tumor. P/M/- showed no difference from no treatment control, indicating that magnetophoretic priming alone had no direct anti-cancer effect at the dose used in this study. As expected from the imaging study (Fig. 2c–e) and tissue evaluation (Fig. 3), P/-/D (i.e., -M) was not as effective as P/M/D (i.e., +M) due to the lack of priming effect, thereby inefficient tumor delivery of Doxil. Importantly, D/P/M regimen was subpar to P/M/D, supporting that the effect of P/M/D was not a simple sum of PTX@PINC and Doxil but a consequence of the improved Doxil delivery by tumor priming. The weights of tumors sampled at 33 d post-inoculation maintained the same rank order (Fig. 4d, Fig. S8). No significant decrease in body weight was observed over 27 d (Fig. S8), indicating minimal toxicity of the treatments. The same experiment was repeated with P/-/D and P/M/D, and a consistent trend was observed (Fig. S10).

3.7. Effect of tumor priming on metastasis of 4T1 tumors

Orthotopic 4T1 tumor model is well-known for high incidence of lung metastasis.[44, 45] Metastatic spread of orthotopic 4T1 tumors is reported to be detectable as early as 8 d post-tumor inoculation.[46, 47] We evaluated the extent of metastasis at the time of sacrifice (33 d post-inoculation) to determine if tumor priming at 10 and 12 d post-inoculation increased the metastasis of 4T1 tumors by depleting stromal containment. The lungs of animals treated with P/M/D showed the least number of metastatic nodules, whereas those of other groups showed a broad range in the number of nodules (Fig. 4e, Fig. S9). We exclude the possibility of differential accumulation of Doxil in the lung because other regimens including Doxil (P/-/D, D/P/M) did not show comparable effects. The attenuation of metastasis is rather likely a secondary effect of the initial Doxil delivery to primary tumors. Given that lung metastasis of 4T1 tumors is observed well after the removal of primary tumor,[47] 4T1 metastasis is thought to occur with the expansion of metastatic foci established at the early stage rather than a continued export of primary tumors.[46] P/M/D regimen applied on 10 and 12 d post-inoculation might have prevented the migration of primary tumors to distant organs at the most critical time, although it did not have a long-lasting effect on primary tumors (Fig. 4d). This result supports that PTX@PINC-mediated tumor priming does not increase but rather suppress the metastatic spread of the primed tumors via efficient delivery of chemotherapy to primary tumors.

4. Conclusion

To facilitate chemotherapy of solid tumors, 4T1 murine breast tumors were primed with magnetophoretically delivered PTX@PINC. The primed tumors developed acellular area at a subtoxic level of PTX and accommodated the subsequently administered NPs better than non-primed tumors. Consequently, the primed tumors responded to Doxil better than non-primed ones, showing delayed growth at the early stage. Moreover, lung metastasis was

significantly reduced in animals receiving PINC-mediated tumor priming, which indicates that the early management of primary tumors was critical to preventing the development of metastatic foci. PINC combined with magnetophoresis provides a useful tool for timed and localized delivery of tumor-priming agents.

Supplementary Material

Refer to Web version on PubMed Central for supplementary material.

Acknowledgments

This work was supported by a Lilly Innovation Fellowship Award, NIH R01 EB017791, NIH R01 CA232419 and the Purdue University Center for Cancer Research (NIH P30 CA023168). We thank the Bindley Imaging Facility at Purdue University for whole body animal image, Dr. Gregory Tamer for technical support with MR imaging and data analysis, and Dr. Henry Havel for discussion of this research.

References

1. Khawar IA; Kim JH; Kuh HJ Improving Drug Delivery to Solid Tumors: Priming the Tumor Microenvironment. J. Control Release 2015, 201, 78–89. [PubMed: 25526702]
2. Gao H Shaping Tumor Microenvironment for Improving Nanoparticle Delivery. Curr. Drug Metab 2016, 17, 731–736. [PubMed: 27396754]
3. Yang S; Gao H Nanoparticles for Modulating Tumor Microenvironment to Improve Drug Delivery and Tumor Therapy. Pharmacol. Res 2017, 126, 97–108. [PubMed: 28501517]
4. Overchuk M; Zheng G Overcoming Obstacles in the Tumor Microenvironment: Recent Advancements in Nanoparticle Delivery for Cancer Theranostics. Biomaterials 2018, 156, 217–237. [PubMed: 29207323]
5. Chauhan VP; Stylianopoulos T; Boucher Y; Jain RK Delivery of Molecular and Nanoscale Medicine to Tumors: Transport Barriers and Strategies. Annu. Rev. Chem. Biomol. Eng 2011, 2, 281–98. [PubMed: 22432620]
6. Helmlinger G; Netti PA; Lichtenbeld HC; Melder RJ; Jain RK Solid Stress Inhibits the Growth of Multicellular Tumor Spheroids. Nat. Biotechnol 1997, 15, 778–83. [PubMed: 9255794]
7. Sun C; Jain RK; Munn LL Non-Uniform Plasma Leakage Affects Local Hematocrit and Blood Flow: Implications for Inflammation and Tumor Perfusion. Ann. Biomed. Eng 2007, 35, 2121–2129. [PubMed: 17846892]
8. Yuan F; Leunig M; Huang SK; Berk DA; Papahadjopoulos D; Jain RK Microvascular Permeability and Interstitial Penetration of Sterically Stabilized (Stealth) Liposomes in a Human Tumor Xenograft. Cancer Res. 1994, 54, 3352–6. [PubMed: 8012948]
9. Magzoub M; Jin S; Verkman AS Enhanced Macromolecule Diffusion Deep in Tumors after Enzymatic Digestion of Extracellular Matrix Collagen and its Associated Proteoglycan Decorin. FASEB J. 2008, 22, 276–84. [PubMed: 17761521]
10. Nikitovic D; Tzardi M; Berdiaki A; Tsatsakis A; Tzanakakis GN Cancer Microenvironment and Inflammation: Role of Hyaluronan. Front. immunol 2015, 6, 169. [PubMed: 25926834]
11. Thompson CB; Shepard HM; O'Connor PM; Kadhim S; Jiang P; Osgood RJ; Bookbinder LH; Li X; Sugarman BJ; Connor RJ; Nadjsombati S; Frost GI Enzymatic Depletion of Tumor Hyaluronan Induces Antitumor Responses in Preclinical Animal Models. Mol. Cancer Ther 2010, 9, 3052–64. [PubMed: 20978165]
12. Hingorani SR; Harris WP; Beck JT; Berdov BA; Wagner SA; Pshevlotsky EM; Tjulandin SA; Gladkov OA; Holcombe RF; Korn R; Raghunand N; Dychter S; Jiang P; Shepard HM; Devoe CE Phase Ib Study of PEGylated Recombinant Human Hyaluronidase and Gemcitabine in Patients with Advanced Pancreatic Cancer. Clin. Cancer Res 2016, 22, 2848–54. [PubMed: 26813359]

13. Kohli AG; Kivimae S; Tiffany MR; Szoka FC Improving the Distribution of Doxil(R) in the Tumor Matrix by Depletion of Tumor Hyaluronan. J. Control. Release 2014, 191, 105–14. [PubMed: 24852095]

14. Diop-Frimpong B; Chauhan VP; Krane S; Boucher Y; Jain RK Losartan Inhibits Collagen I Synthesis and Improves the Distribution and Efficacy of Nanotherapeutics in Tumors. Proc. Natl. Acad. Sci. U S A 2011, 108, 2909–14. [PubMed: 21282607]

15. Goldman A; Kulkarni A; Kohandel M; Pandey P; Rao P; Natarajan SK; Sabbisetti V; Sengupta S Rationally Designed 2-in-1 Nanoparticles Can Overcome Adaptive Resistance in Cancer. ACS nano 2016, 10, 5823–34. [PubMed: 27257911]

16. Davies Cde L; Lundstrom LM; Frengen J; Eikenes L; Bruland SO; Kaalhus O; Hjelstuen MH; Brekken C Radiation Improves the Distribution and Uptake of Liposomal Doxorubicin (Caelyx) in Human Osteosarcoma Xenografts. Cancer Res. 2004, 64, 547–53. [PubMed: 14744768]

17. Zhang L; Li R; Chen H; Wei J; Qian H; Su S; Shao J; Wang L; Qian X; Liu B Human Cytotoxic T-Lymphocyte Membrane-Camouflaged Nanoparticles Combined with Low-Dose Irradiation: a New Approach to Enhance Drug Targeting in Gastric Cancer. Int. J. Nanomedicine 2017, 12, 2129–2142. [PubMed: 28360520]

18. Appelbe OK; Zhang Q; Pelizzari CA; Weichselbaum RR; Kron SJ Image-Guided Radiotherapy Targets Macromolecules through Altering the Tumor Microenvironment. Mol. Pharm 2016, 13, 3457–3467. [PubMed: 27560921]

19. Sugahara KN; Teesalu T; Karmali PP; Kotamraju VR; Agemy L; Girard OM; Hanahan D; Mattrey RF; Ruoslahti E Tissue-Penetrating Delivery of Compounds and Nanoparticles into Tumors. Cancer Cell 2009, 16, 510–520. [PubMed: 19962669]

20. Sugahara KN; Teesalu T; Karmali PP; Kotamraju VR; Agemy L; Greenwald DR; Ruoslahti E Coadministration of a Tumor-Penetrating Peptide Enhances the Efficacy of Cancer Drugs. Science 2010, 328, 1031–1035. [PubMed: 20378772]

21. Jang SH; Wientjes MG; Au JL Enhancement of Paclitaxel Delivery to Solid Tumors by Apoptosis-Inducing Pretreatment: Effect of Treatment Schedule. J. Pharmacol. Exp. Ther 2001, 296, 1035–42. [PubMed: 11181938]

22. Lu D; Wientjes MG; Lu Z; Au JL Tumor Priming Enhances Delivery and Efficacy of Nanomedicines. J. Pharmacol. Exp. Ther 2007, 322, 80–8. [PubMed: 17420296]

23. Von Hoff DD; Ramanathan RK; Borad MJ; Laheru DA; Smith LS; Wood TE; Korn RL; Desai N; Trieu V; Iglesias JL; Zhang H; Soon-Shiong P; Shi T; Rajeshkumar NV; Maitra A; Hidalgo M Gemcitabine Plus Nab-Paclitaxel is an Active Regimen in Patients with Advanced Pancreatic Cancer: a Phase I/II Trial. J. Clin. Oncol2011, 29, 4548–54. [PubMed: 21969517]

24. Gore J; Korc M Pancreatic Cancer Stroma: Friend or Foe? Cancer Cell 2014, 25, 711–2. [PubMed: 24937454]

25. Rhim AD; Oberstein PE; Thomas DH; Mirek ET; Palermo CF; Sastra SA; Dekleva EN; Saunders T; Becerra CP; Tattersall IW; Westphalen CB; Kitajewski J; Fernandez-Barrena MG; Fernandez-Zapico ME; Iacobuzio-Donahue C; Olive KP; Stanger BZ Stromal Elements Act to Restrain, Rather Than Support, Pancreatic Ductal Adenocarcinoma. Cancer Cell 2014, 25, 735–47. [PubMed: 24856585]

26. Ozdemir BC; Pentcheva-Hoang T; Carstens JL; Zheng X; Wu CC; Simpson TR; Laklai H; Sugimoto H; Kahlert C; Novitskiy SV; De Jesus-Acosta A; Sharma P; Heidari P; Mahmood U; Chin L; Moses HL; Weaver VM; Maitra A; Allison JP; LeBleu VS; Kalluri R Depletion of Carcinoma-Associated Fibroblasts and Fibrosis Induces Immunosuppression and Accelerates Pancreas Cancer with Reduced Survival. Cancer Cell 2014, 25, 719–34. [PubMed: 24856586]

27. Park J; Kadasala NR; Abouelmagd SA; Castanares MA; Collins DS; Wei A; Yeo Y Polymer-Iron Oxide Composite Nanoparticles for EPR-Independent Drug Delivery. Biomaterials 2016, 101, 285–95. [PubMed: 27310916]

28. Paschall AV; Liu K An Orthotopic Mouse Model of Spontaneous Breast Cancer Metastasis. J. Vis. Exp 2016, 114, 54040.

29. Gabizon A; Tzemach D; Mak L; Bronstein M; Horowitz AT Dose Dependency of Pharmacokinetics and Therapeutic Efficacy of Pegylated Liposomal Doxorubicin (DOXIL) in Murine Models. J. Drug Target 2002, 10, 539–48. [PubMed: 12683721]

30. Euhus DM; Hudd C; LaRegina MC; Johnson FE Tumor Measurement in the Nude Mouse. J. Surg. Oncol 1986, 31, 229–34. [PubMed: 3724177]

31. Mehrara E; Forssell-Aronsson E; Ahlman H; Bernhardt P Specific Growth Rate Versus Doubling Time for Quantitative Characterization of Tumor Growth Rate. Cancer Res. 2007, 67, 3970–5. [PubMed: 17440113]

32. Filardi MJ; Lininger L; McKneally MF Adaptation of an Automatic Bacterial Colony Counter for Measuring Lung Tumor Growth in Mice. Cancer Res. 1977, 37, 2726–8. [PubMed: 326389]

33. Wexler H; Chretien PB; Ketcham AS; Sindelar WF Induction of Pulmonary Metastases in Both Immune and Nonimmune Mice. Effect of the Removal of a Transplanted Primary Tumor. Cancer 1975, 36, 2042–7. [PubMed: 1203862]

34. Dong S; Maziveyi M; Alahari SK Primary Tumor and MEF Cell Isolation to Study Lung Metastasis. J. Vis. Exp 2015, e52609. [PubMed: 26066699]

35. Liu Y; Ai K; Lu L Polydopamine and Its Derivative Materials: Synthesis and Promising Applications in Energy, Environmental, and Biomedical Fields. Chem. Rev 2014, 114, 5057–115. [PubMed: 24517847]

36. Xu C; Xu K; Gu H; Zheng R; Liu H; Zhang X; Guo Z; Xu B Dopamine as a Robust Anchor to Immobilize Functional Molecules on the Iron Oxide Shell of Magnetic Nanoparticles. J. Am. Chem. Soc 2004, 126, 9938–9939. [PubMed: 15303865]

37. Shultz MD; Reveles JU; Khanna SN; Carpenter EE Reactive Nature of Dopamine as a Surface Functionalization Agent in Iron Oxide Nanoparticles. J. Am. Chem. Soc 2007, 129, 2482–2487. [PubMed: 17290990]

38. Park J; Brust TF; Lee HJ; Lee SC; Watts VJ; Yeo Y Polydopamine-Based Simple and Versatile Surface Modification of Polymeric Nano Drug Carriers. ACS Nano 2014, 8, 3347–3356. [PubMed: 24628245]

39. Lee H; Dellatore SM; Miller WM; Messersmith PB Mussel-Inspired Surface Chemistry for Multifunctional Coatings. Science 2007, 318, 426–430. [PubMed: 17947576]

40. Hyun H; Park J; Willis K; Park JE; Lyle LT; Lee W; Yeo Y Surface Modification of Polymer Nanoparticles with Native Albumin for Enhancing Drug Delivery to Solid Tumors. Biomaterials 2018, 180, 206–224. [PubMed: 30048910]

41. Han N; Pang L; Xu J; Hyun H; Park J; Yeo Y Development of Surface-Variable Polymeric Nanoparticles for Drug Delivery to Tumors. Mol. Pharm 2017, 14, 1538–1547. [PubMed: 28368124]

42. Makadia HK; Siegel SJ Poly Lactic-co-Glycolic Acid (PLGA) as Biodegradable Controlled Drug Delivery Carrier. Polymers 2011, 3, 377–1397.

43. Xu P; Gullotti E; Tong L; Highley CB; Errabelli DR; Hasan T; Cheng JX; Kohane DS; Yeo Y Intracellular Drug Delivery by Poly(Lactic-Co-Glycolic Acid) Nanoparticles, Revisited. Mol. Pharm 2009, 6, 190–201. [PubMed: 19035785]

44. Gomez-Cuadrado L; Tracey N; Ma R; Qian B; Brunton VG Mouse Models of Metastasis: Progress and Prospects. Dis. Model Mech 2017, 10, (9), 1061–1074. [PubMed: 28883015]

45. Pulaski BA; Ostrand-Rosenberg S Mouse 4T1 Breast Tumor Model. Curr. Protoc. Immunol 2001, Chapter 20, Unit 20.2.

46. DuPre SA; Redelman D; Hunter KW Jr. The Mouse Mammary Carcinoma 4T1: Characterization of the Cellular Landscape of Primary Tumours and Metastatic Tumour Foci. Int. J. Exp. Pathol 2007, 88, 351–60. [PubMed: 17877537]

47. Kershaw MH; Jackson JT; Haynes NM; Teng MWL; Moeller M; Hayakawa Y; Street SE; Cameron R; Tanner JE; Trapani JA; Smyth MJ; Darcy PK Gene-Engineered T Cells as a Superior Adjuvant Therapy for Metastatic Cancer. J. Immunol 2004, 173, 2143–2150. [PubMed: 15265951]

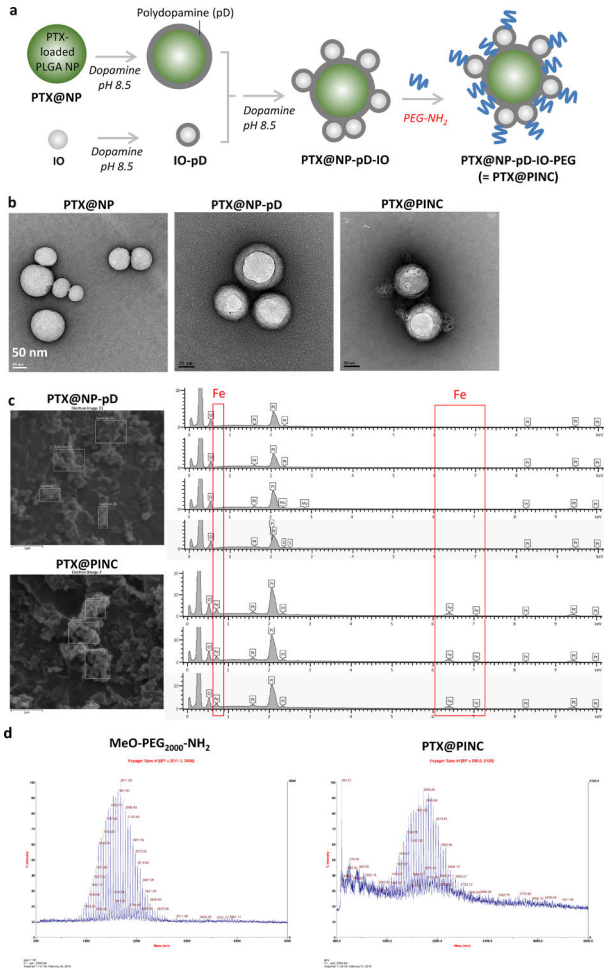

Fig. 1.

(a) Schematic of PTX@PINC preparation; (b) transmission electron microscopy images of PTX@NP, PTX@NP-pD, and PTX@PINC. Scale bars: 50 nm. (c) SEM-EDX analysis of PTX@NP-pD and PTX@PINC. The latter shows Fe signals from the surface-bound iron oxide particles. (d) MALDI-MS analysis of MeO-PEG_{2000}-NH_2 and PTX@PINC. Larger scale figures are shown in Figure S1.

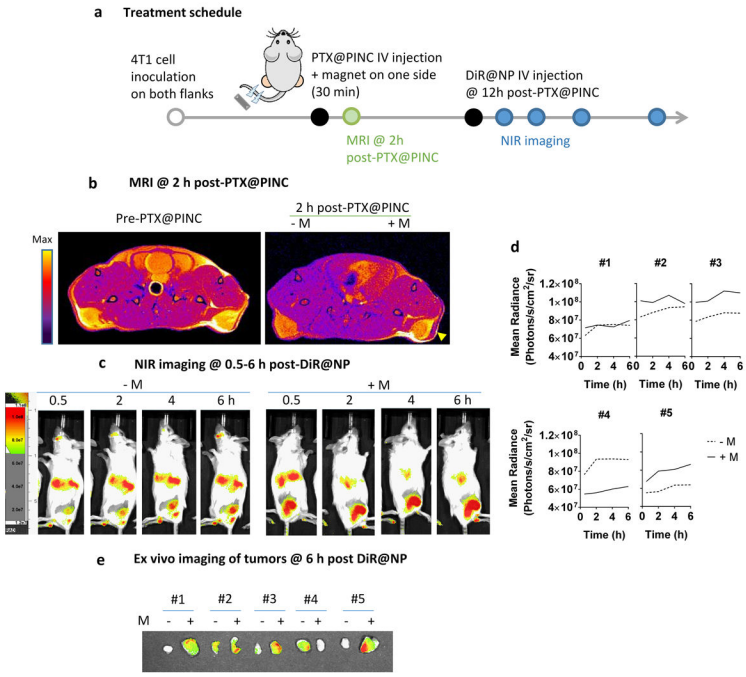

Fig. 2.

(a) Treatment and imaging schedule; (b) representative T2-weighted MR images of a 4T1 tumor-bearing Balb/c female mouse before and after the injection of PTX@PINC with or without a magnet exposure (± M); (c) near infrared fluorescence whole body images after DiR@NP injection following tumor priming with PTX@PINC +M; (d) DiR intensity of tumor of each animal; (e) photograph of *ex vivo* 4T1 tumors, excised at 6 h after DiR@NP injection (n=5).

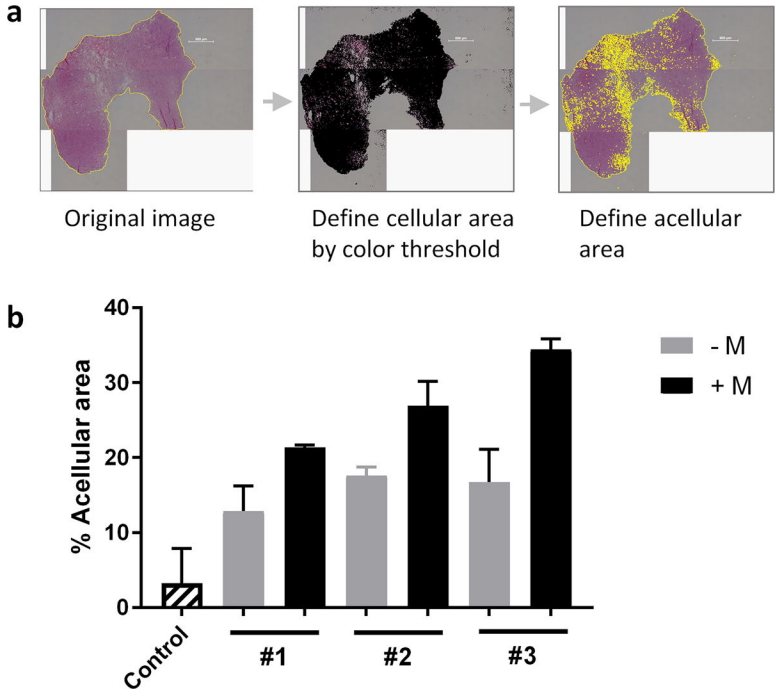

Fig. 3.

(a) Image analysis scheme: Acellular area in each tumor section was defined by Image J; (b) % acellular area = acellular area / total tumor area × 100. #1, #2, and #3 are mouse identity. 6–12 images were stitched together to make one section image. Data indicates mean ± s.d. of two to three section images per each side (± M) per mouse. The image in (a) panel is from mouse #1. For images of tumor sections from all three mice, see Figure S7.

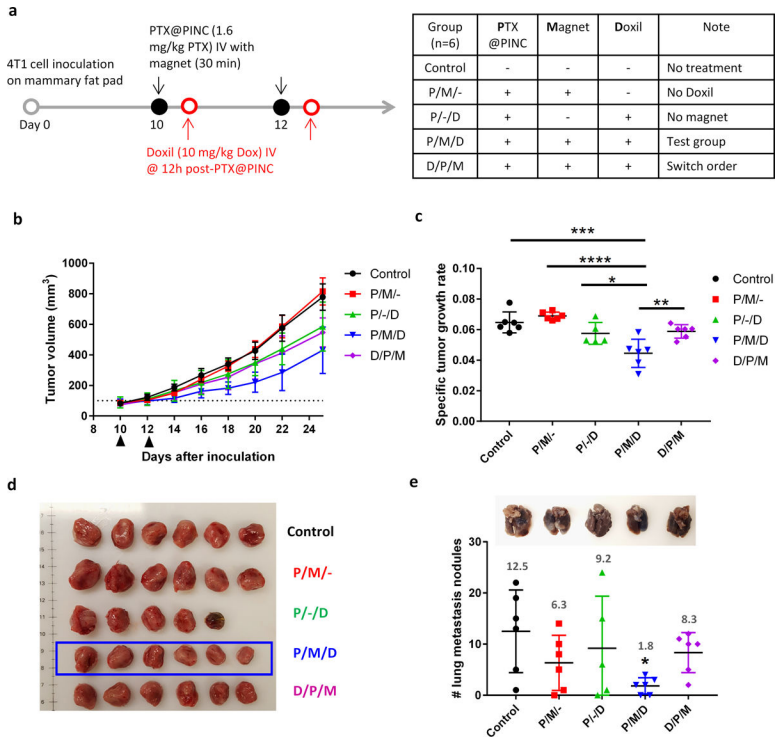

Group (n=6)	PTX @PINC	Magnet	Doxil	Note
Control	-	-	-	No treatment
P/M/-	+	+	-	No Doxil
P/-/D	+	-	+	No magnet
P/M/D	+	+	+	Test group
D/P/M	+	+	+	Switch order

Fig. 4.

Antitumor efficacy of Doxil administered after tumor-priming. (a) Treatment schedule and regimen; (b) tumor volume change after 2 consecutive treatments; (c) specific tumor growth rates of 4T1 tumors after the treatment. $\Delta \log V/\Delta t$ (V: tumor volumes; t: time in days). *: $p < 0.05$; **: $p < 0.01$; ***: $p < 0.001$ by ordinary One-way ANOVA followed by Tukey's multiple comparisons test; (d) photograph of 4T1 tumors, excised on 33 d post-inoculation; (e) number of metastasis nodules in the lungs. *: $p < 0.05$ by Kruskal-Wallis One-way ANOVA. n = 5–6 per group.

Table 1.

Particle sizes of PTX@NP, PTX@NP-pD, and PTX@PINC

	Z-average[a] (d, nm)	Number mean diameter (nm)	PDI[b]	PTX content (wt%)	Fe content (wt%)
PTX@NP	183.1 ± 1.9	141.0 ± 9.5	0.07 ± 0.02	2.5 ± 0.3	Not applicable
PTX@NP-pD	186.0 ± 0.9	132.2 ± 5.2	0.1 ± 0.01	Not available	Not applicable
PTX@PINC	262 ± 37	207 ± 41	0.14 ± 0.03	1.6 ± 0.5	2.3 ± 0.6

Core NPs were prepared with PLGA (30 kDa, LA:GA=85:15).

Data: mean ± standard deviation of 5–6 independently and identically prepared batches

[a] Z-averages were measured assuming that the particles were spherical.

[b] Polydispersity index (PDI) was obtained by cumulant analysis as described in the International Standard on DLS ISO13321 Part 8 (Malvern DLS technical note MRK656–01).